Proceedings of "Applications of Physics in Mechanical and Material Engineering" (APMME 2024)

Impact of Aluminum Addition on Microstrain and Dislocation Density in CoCrFeMnNi High-Entropy Alloys

N.I.M. Ali[a], N.I.M. Nadzri[b,*],
A.A.M. Salleh[a], A.S. Sangar[a],
T.-S. Jun[b] and S. Joseph[c]

[a] *Centre of Excellence Geopolymer and Green Technology (CEGeoGTech), Faculty of Chemical Engineering Technology, Universiti Malaysia Perlis (UniMAP), Taman Muhibbah, 02600 Arau, Perlis, Malaysia*
[b] *Department of Mechanical Engineering, Incheon Univeristy, 119 Academy-ro, Songdo-dong, Teonsu-gu, Incheon 22012, Republic of Korea*
[c] *Department of Materials Engineering, Cambridge Institute of Technology, Bengaluru, Karnataka 560036, India*

Doi: 10.12693/APhysPolA.147.266 *e-mail: izzatinadzri@unimap.edu.my

In this research, the influence of aluminum (Al) addition on the structural and mechanical properties of CoCrFeMnNi high-entropy alloys was investigated through the lens of solid-state physics. Utilizing vacuum arc melting for fabrication, the study examines the phase transformations, lattice distortions, and their correlation with material hardness. X-ray diffraction analysis reveals a 2.5% peak shift from 44.55° (face-centered cubic) to 45.66° (body-centered cubic), indicating a phase transition. This structural evolution is accompanied by a 142.7% increase in microstrain (from 1.44×10^{-5} to 3.48×10^{-5}) and a 58.6% rise in dislocation density (from 4.06×10^{7} to 6.44×10^{7} cm^{-2}), signifying enhanced lattice distortions. Consequently, the Vickers hardness improves by 178.3%, from 183.38 ± 5 to 510.59 ± 5 HV. The transition from face-centered phase to body-centered cubic phase, driven by lattice distortions and microstructural modifications, underscores the Al's pivotal role in optimizing HEA properties. These findings provide critical insights into the phase behavior and mechanical property enhancement, contributing to advances in the design and application of high-performance materials.

topics: high-entropy alloys (HEAs), X-ray diffraction (XRD)

1. Introduction

High entropy alloys (HEAs) can be defined as solid solutions of five or more metals mixed in nearly equimolar proportions [1–5]. One of the key characteristics of HEAs is that their configurational entropy (ΔS_{config}) is typically close to or greater than $1.5R$, where R represents the universal gas constant. There are four main effects in HEA: thermodynamics (high entropy effect), kinetics (sluggish diffusion), structures (severe lattice distortion), and properties (cocktail effects) [6, 7]. Nowadays, researchers frequently investigate the HEAs' unique structure and physical properties, e.g., alloys with high wear-resistant, high strength at room temperature or elevated temperatures, and general corrosion resistance much better than conventional alloys. Among HEAs, the equiatomic CoCrFeMnNi alloy has attracted significant attention due to its single-phase face-centered cubic (FCC) structure and remarkable toughness [8–10].

The addition of aluminium (Al) has shown potential in altering phase stability and inducing lattice distortions, leading to structural transformations and improved mechanical performance [11–13]. Al addition often stabilizes body-centered cubic (BCC) phases, affecting microstrain, dislocation density, and hardness. Understanding these structural changes is crucial for tailoring HEAs for advanced engineering applications.

In this paper, we show the results of microstrain, dislocation density, and hardness of Al addition in CoCrFeMnNi HEA, using X-ray diffraction (XRD) and Vickers hardness testing. Based on them, we elucidate the role of Al in phase transitions and lattice distortions, bridging the gap between structural physics and mechanical performance.

2. Experimental procedure

High entropy CoCrFeMnNi and CoCrFeMnNiAl alloys were prepared by vacuum arc melting technique. Equiatomic amount of Co, Cr, Fe, Mn, Ni, and Al (minimum purity of 99%) was melted and remelted several times to increase homogeneity. The molten metal was poured into $250 \times 20 \times 25$ mm^3 mould. To facilitate the measurement, the sample was cut using a band saw.

The crystal structure was examined by a XRD Shimadzu 6000 diffractometer. Tests were conducted on polished specimens for diffraction angles ranging from 20° to 80°. The Cu K_α source ($\lambda = 1.5406$ Å) was set. The obtained XRD patterns were analyzed using the Panaltical HighScore Plus software. The microstrain (ε) and dislocation (δ) are derived from the Williamson–Hall method [14], i.e.,

$$\varepsilon = \left(\frac{\text{FWHM [rad]}}{4 \tan\left(\frac{\pi\theta}{180}\right)} \right)^2 \tag{1}$$

$$\delta = \left(\frac{\text{FWHM [rad]}}{4 \tan\left(\frac{\pi\theta}{180}\right)} \right)^{-1}, \tag{2}$$

where FWHM is the width of the XRD peak at half of its maximum intensity [rad], θ is the Bragg's angle [°].

The hardness measurement was performed by using a Sinowon WH series Digital Auto-Turret Vickers Hardness Tester with a Vickers indenter with a load of 0.1 kgf.

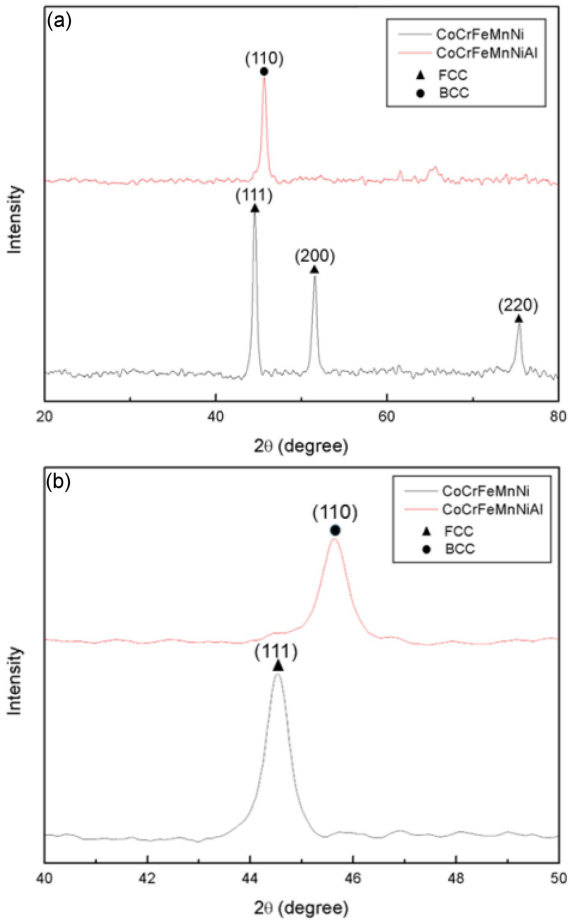

Fig. 1. Result of X-ray diffraction patterns of CoCrFeMnNi and CoCrFeMnNiAl HEA. Black and red lines represent CoCrFeMnNi and CoCrFeMnNiAl HEA, respectively. (a) Overall XRD patterns and (b) main peaks of patterns.

3. Results

Figure 1 shows the XRD pattern obtained for CoCrFeMnNi and CoCrFeMnNiAl HEA.

The analysis of the XRD pattern indicates the presence of two major phases in which CoCrFeMnNi crystallizes in a face-centered cubic (FCC) structure with lattice parameter $a = 3.589$ Å (space group $Fm{-}3m$). In turn, CoCrFeMnNiAl crystallizes in a body-centered cubic (BCC) structure with lattice parameter $a = 5.770$ Å (space group ($Fm{-}3m$). CoCrFeMnNi alloy exhibits smaller lattice parameters due to the compact structure of FCC crystal structure as compared to CoCrFeMnNiAl alloy. The increase in lattice parameter is caused by the larger atomic radius of Al (143 pm) as compared to constituent elements like Cr (128 pm), Fe (126 pm), Co (125 pm), Mn (127 pm), and Ni (124 pm) [15–17]. This result is further proven by the interplanar spacing (d–d spacing), where there is a slight decrease in d spacing for CoCrFeMnNiAl HEA from 2.0731×10^{-10} to 2.03874×10^{-10} m, indicating closer atomic packing due to the addition of Al. The transition in the alloy's crystalline structure from FCC to BCC structure alters the d spacing due to the fact that different crystal structures have distinct interplanar distances. The incorporation of Al changes the bonding characteristics and interactions as the structure stabilizes into a denser arrangement [18, 19].

The diffraction peaks observed at approximately 44.55°, 51.59°, and 75.48° on the 2θ axis correspond to the (111), (200), and (220) planes of the FCC structure. In contrast, a diffraction peak at around 45.66° was attributed to the (110) plane of the BCC structure. For the CoCrFeMnNi HEA, all the diffraction peaks were identified as part of a single FCC phase. However, with the addition of Al, a new diffraction peak at 45.66° emerged, indicating the formation of the BCC phase. Notably, the FCC peaks completely disappeared in the CoCrFeMnNiAl HEA, leaving only the BCC peaks. The addition of Al also caused a 2.5% peak shift to higher 2θ values, from 44.55° to 45.66°. This shift and transformation from FCC to BCC can be attributed to the lattice distortion induced by

TABLE I

Microstrain and dislocation of Corene and CoCrFeMnNiAl HEAs.

Samples	Microstrain [$\mu\varepsilon$]	Dislocation density [cm^{-2}]
CoCrFeMnNi	1.44×10^{-5}	4.06×10^{7}
CoCrFeMnNiAl	3.48×10^{-5}	6.44×10^{7}

TABLE II

Hardness Vickers and standard deviation values of CoCrFeMnNi and CoCrFeMnNiAl HEAs.

Samples	Hardness Vickers (HV)	Standard deviation
CoCrFeMnNi	183.38	12.43
CoCrFeMnNiAl	510.59	23.66

the larger atomic size of Al. The increased atomic size mismatch generated significant lattice distortion, resulting in peak shifts and structural changes as the lattice adjusted to accommodate the larger Al atoms.

Table I presents the dislocation density and microstrain values for CoCrFeMnNi and CoCrFeMnNiAl HEAs. The microstrain of both samples was calculated using (1). The microstrain in CoCrFeMnNiAl is 2.4 times higher than in CoCrFeMnNi — a significant increase attributed to the addition of Al. The larger atomic radius of Al induces lattice distortion, causing strain at the atomic level, which alters the local atomic environment and results in increased microstrain within the crystal lattice. The addition of equimolar Al also leads to a phase transition from FCC to BCC structure. This transformation further intensifies the lattice distortion due to the difference in atomic packing efficiency between the two phases [19, 20].

The dislocation density of the samples was calculated using (2). The dislocation density of CoCrFeMnNiAl is 1.59 times higher than that of CoCrFeMnNi. The increase in lattice distortions also leads to a higher density of dislocations. The crystal adjusts to accommodate Al atoms due to the difference in atomic radius, which causes lattice strain and elastic distortions. The transition from FCC to BCC crystal structure also results in higher dislocation generation, as the BCC structure has a lower atomic packing factor (0.68) compared to FCC (0.74) [21–23]. This result further supports the idea that the lattice undergoes deformation, promoting the formation of dislocations to relieve internal stresses.

Table II shows the hardness test results and standard deviation values of CoCrFeMnNi and CoCrFeMnNiAl HEAs. The hardness of CoCrFeMnNiAl is higher than CoCrFeMnNi HEA. It correlates to dislocation density — higher dislocation density increases hardness due to dislocation strengthening mechanisms. The dislocation hinders further dislocation movement. Lattice distortions also affect the increase in hardness as the material resists deformation under the applied load. Higher microstrain contributes to hardening as the material becomes more resistant to deformation due to internal stresses created by lattice mismatch. This is evident in the higher hardness of CoCrFeMnNiAl. A higher standard deviation of CoCrFeMnNiAl suggests more variability in hardness, which may be due to increased dislocation density and microstrain, which cause local variations in hardness across the material. Schön et al. [7] stated that larger atomic radius of Al and phase transition from FCC to BCC contribute to solid solution strengthening of alloys, making the alloy resistant to dislocation motion. Combined with the microstrain and dislocation density, it leads to a significant increase in hardness, which proves that the Al addition plays a critical role in enhancing the mechanical properties of CoCrFeMnNi HEA [23].

4. Conclusions

In this study, the structural and mechanical properties of CoCrFeMnNi and CoCrFeMnNiAl HEAs were examined. XRD analysis revealed that the addition of aluminium (Al) to CoCrFeMnNi high-entropy alloys (HEAs) induces a phase transition from a face-centered cubic (FCC) to a body-centered cubic (BCC) structure. The larger atomic radius of Al (143 pm) compared to other elements in the alloy and the transition from FCC to BCC phase resulted in increased lattice distortion, microstrain, and dislocation density. These changes contribute to the significant increase in hardness for CoCrFeMnNiAl compared to CoCrFeMnNi. Additionally, the higher standard deviation in hardness for CoCrFeMnNiAl suggests a larger variability, likely due to increased dislocation density and microstrain. These findings highlight the significant role of Al in altering the microstructure and mechanical properties of CoCrFeMnNi HEAs.

Acknowledgments

The authors gratefully acknowledge the support provided by the Fundamental Research Grant Scheme under grant no. FRGS/1/2022/STG05/UNIMAP/02/3 funded by the Ministry of Education Malaysia, Center of Excellence Geopolymer & Green Technology (CEGeoGTech), Faculty of Chemical Engineering and Technology, Universiti Malaysia Perlis (UniMAP).

References

[1] Y. Duan, M. Li, Y. Guo, N. Zhu, H. Pang, C. Dou, *Mater. Today Phys.* **49**, 101596 (2024).

[2] K.X. Yin, G.Y. Dong, G.J. Zhang, Q.W. Tian, Y.N. Wang, J.C. Huang, *J. Mater. Res. Technol.* **24**, 7654 (2023).

[3] B. Jin, N. Zhang, B. Xing, N. Fan, S. Nie, X. Wang, S. Yin, X. Zhu, *Mater. Charact.* **205**, 113233 (2023).

[4] L. Chen, *Arch. Metall. Mater.* **68**, 881 (2023).

[5] S.-Y. Park, J.P. Park, K.-A. Lee, *Arch. Metall. Mater.* **69**, 447 (2024).

[6] V. Balaji, P. Jeyapandiarajan, J. Joel, A. Anbalagan, P. Ashwath, S.M. Anouncia, A. Batako, M.A. Xavior, *J. Mater. Res. Technol.* **33**, 7681 (2024).

[7] C.G. Schön, M.A. Tunes, R. Arróyave, J. Ågren, *Calphad* **68**, 101713 (2020).

[8] H. Feng, Y. Han, H.-B. Li, Y.-Z. Tian, H.-C. Zhu, Z.-H. Jiang, T. He, G. Zhou, *J. Alloys Compd.* **932**, 167615 (2023).

[9] J. Agyapong, D. Mateos, A. Czekanski, S. Boakye-Yiadom, *J. Alloys Compd.* **987**, 173998 (2024).

[10] S. Konovalov, S. Gudala, I. Panchenko, K. Osintsev, X. Chen, *Vacuum* **227**, 113405 (2024).

[11] K. Zhou, W. Yu, B. Ren, G. Wang, P. Yao, *Mater. Charact.* **216**, 114278 (2024).

[12] X. An, F. Li, L. Kan et al., *Mater. Chem. Phys.* **328**, 129988 (2024).

[13] S. Salifu, P.A. Olubambi, L. Teffo, *Heliyon* **10**, e24498 (2024).

[14] M. Rabiei, A. Palevicius, A. Dashti, S. Nasiri, A. Monshi, A. Doustmohammadi, A. Vilkauskas, G. Janusas, *Materials* **14**, 2949 (2021).

[15] H. Lee, A. Sharma, B. Ahn, *J. Alloys Compd.* **947**, 169545 (2023).

[16] S. Chen, Y. Tan, X. Wang, F. Cao, L. Wang, Y. Su, J. Guo, *J. Mater. Res. Technol.* **23**, 209 (2023).

[17] W.C. Kim, M.Y. Na, H.J. Kwon, Y.S. Na, J.W. Won, H.J. Chang, K.R. Lim, *Acta Mater.* **211**, 116890 (2021).

[18] C.-S. Wu, P.-H. Tsai, C.-M. Kuo, C.-W. Tsai, *Entropy* **20**, 12 (2018).

[19] Y.-C. Hsu, C.-L. Li, C.-H. Hsueh, *Entropy* **22**, 1 (2019).

[20] Z. Peng, Z. Fan, M.R. Abdullah, C. Ren, J. Li, P. Gong, *Materials* **16**, 13 (2023).

[21] R.K. Nutor, Q. Cao, X. Wang, D. Zhang, Y. Fang, Y. Zhang, J.-Z. Jiang, *Adv. Eng. Mater.* **22**, 2000466 (2020).

[22] A.A. Sasikala Devi, V. Javaheri, S. Pallaspuro, J. Komi, *Phys. Chem. Chem. Phys.* **26**, 26222 (2024).

[23] M. Kozejova, R. Bodnarova, V. Latyshev, M. Lisnichuk, V. Girman, H. You, V. Komanicky, *Int. J. Hydrogen Energy* **47**, 26987 (2022).